Characterizing carrier envelope phase of an isolated attosecond pulse with annular photoionization momentum spectra

Meng Li (李 猛)[1,2], Guizhong Zhang (张贵忠)[1,*], Tianqi Zhao (赵天琪)[1], Xin Ding (丁 欣)[1], and Jian Yao (姚键铨)[1]

[1]*College of Precision Instrument and Optoelectronics Engineering, Tianjin University, Tianjin 300072, China*
[2]*Civil Aviation Meteorological Institute, Key Laboratory of Operation Programming and Safety Technology of Air Traffic Management, Civil Aviation University of China, Tianjin 300300, China*
**Corresponding author: johngzhang@tju.edu.cn*

Received April 13, 2017; accepted July 28, 2017; posted online September 8, 2017

The carrier envelope phase (CEP) has a direct impact on the physical properties of an isolated attosecond pulse (IAP) and many strong field processes, but it is difficult to measure in reality. Aiming at obtaining more accurate and complete characterization of CEP, we numerically investigate the annular photoelectron momentum spectra of the hydrogen atom ionized by overlapped fields of an IAP and an infrared (IR) pulse. By defining an overlapping parameter, the momentum patterns are classified and optimized for unambiguously measuring the rotation angle of a momentum pattern versus the CEP value. A series of simulations verify its robustness.

OCIS codes: 020.2649, 020.1335.
doi: 10.3788/COL201715.110201.

Isolated attosecond pulse (IAP), first proposed in 2001[1], detects the photoelectron energy distribution by combining an intense ultrashort infrared (IR) pulse and a attosecond extreme ultraviolet (XUV) pulse. Supercontinuum high harmonics is applied to obtain the few-cycle IAP[2]. Deploying IAP, one can perform the attosecond control of electronic processes[2–5], and investigate the dynamics of atoms and molecules at the attosecond level, opening the door to understand the microscopic world more accurately. Many fundamental parameters, such as wavelength, pulse duration, intensity, and carrier envelope phase (CEP), determine and affect the performance of an IAP. Compared to other parameters, however, owing to the far weak intensity of an IAP, the CEP is more difficult to capture and characterize[6]. As a crucial parameter, a stable CEP has a substantial impact on the optical frequency measurement[7] and many microscopic detection approaches, such as the attosecond streak camera[8], attosecond measurement[9], and the electron localization[10]. Therefore, a series of approaches have been proposed to describe the CEP[11–17] over the past few decades. Initially, Paulus[18] proposed a CEP-measuring method for few-cycle laser pulses on the basis of strong interaction between laser and atoms. This method has led to the significant ideas that the characteristics of photoionized atoms can be profoundly affected by the CEP. Later on, other approaches[19–22] based on tunneling ionization were also demonstrated, most of which focused principally on the properties of photoelectron momentum pattern[23,24] induced by the CEP variation. For instance, Wittmann *et al.*[19] utilized the left–right asymmetries of photoelectrons emitted along the laser polarization to detect the CEP information. These techniques are suitable to CEP description of few-cycle laser pulses; however, they become less powerful in determining the CEP of an IAP because of the weak nonlinear process that induced the IAP. In recent years, people have been focusing on the CEP measurement of an IAP, and have developed a few[25,26] pulse-combination strategies to generate momentum or energy spectra. The idea was first presented in 2010[25], where an intense few-cycle IR pulse and an IAP were superimposed to ionize a molecule, and the CEP was encrypted in the quantum mechanical interference of the momentum pattern. Similarly, Liu *et al.*[27] proposed a method of two-color photoionization where a CEP-stabilized IR pulse and an attosecond waveform were combined to generate the coherent photoelectron spectra to get the CEP of an IAP. The essence of these methods lies in amplifying the effect of the CEP of an IAP by coherent superposition, but the prerequisite is a strictly stable CEP. In addition, the CEP description was also proposed with momentum angular streaking[28]. This approach employed circularly polarized superimposed[29,30] IAP and an IR pulse to ionize atoms, and characterized the CEP by the photoelectron momentum spectra[31–33], thus opening the possibility of detecting the CEP of a weak IAP accurately with an IR pulse. However, the significant effect due to the overlapping position of the IAP with the IR pulse was not considered, which impairs the performance of the proposed CEP description.

In this Letter, we demonstrate an improved approach of the IAP CEP characterization by deploying the rotation of annular photoelectron spectra. This approach not only considers the circular polarization of superimposed pulses of the IAP+IR fields, but also counts the overlapping position of the IAP with the IR pulse as a key parameter.

To this end, we perform extensive numerical simulation and unveil the optimal overlapping position, which induces the most prominent atomic ionization. The thus generated annular photoelectron spectra are suitable for accurate characterization of the IAP CEP.

As a classical approximation, the combination of an IAP and an IR pulse has been widely employed to induce and observe a variety of strong field phenomena, such as Auger decay[34], the tunneling process[35], time delay in photoionization[36], and so on. In our strategy, the IAP and CEP-stabilized IR pulse are both circularly polarized[37,38] and are expressed as

$$\begin{cases} \overrightarrow{E}_{\mathrm{IAP}}(t) = E_{0,\mathrm{IAP}}[\cos(\omega_{\mathrm{IAP}}t+\theta)\hat{x} - \sin(\omega_{\mathrm{IAP}}t+\theta)\hat{y}]\cos^2\left(\pi\frac{t}{\tau_{\mathrm{IAP}}}\right),\ t_1 < t < t_2 \\ \overrightarrow{E}_{\mathrm{IR}}(t) = E_{0,\mathrm{IR}}[\cos(\omega_{\mathrm{IR}}t+\theta_{\mathrm{IR}})\hat{x} - \sin(\omega_{\mathrm{IR}}t+\theta_{\mathrm{IR}})\hat{y}]\cos^2\left(\pi\frac{t}{\tau_{\mathrm{IR}}}\right),\ t_3 < t < t_4 \\ \overrightarrow{E} = \overrightarrow{E}_{\mathrm{IR}} + \overrightarrow{E}_{\mathrm{IAP}} \end{cases} . \tag{1}$$

The square of cosine is the envelope function. The peak field amplitudes $E_{0,\mathrm{IR}}$ and $E_{0,\mathrm{IAP}}$ can be calculated according to $E_0 = (I/3.51\times10^{16})^{1/2}$. θ and θ_{IR} denote the CEPs of the IAP and IR pulse, respectively. t_1, t_2, t_3, and t_4 are the time instants of the IAP and IR pulse. Note that $t_1 > t_3$, and $t_4 > t_2$ for satisfying the overlapping condition. In our simulation, the wavelengths of the IAP and IR pulse are 67 and 800 nm, respectively. The corresponding carrier frequencies are 0.68 and 0.057 a.u., respectively. The superimposed electric field $\overrightarrow{E}$ rotates clockwise in the x–y plane, inducing a photoelectron momentum spectrum when ionizing the hydrogen atom.

As illustrated in Fig. 1, the four time instants t_1, t_2, t_3, and t_4 are applied to describe the overlapping positions of the IAP and IR pulse by defining an overlapping parameter η:

$$\eta = \frac{|t_3 + t_4 - t_1 - t_2|}{t_4 - t_3}. \tag{2}$$

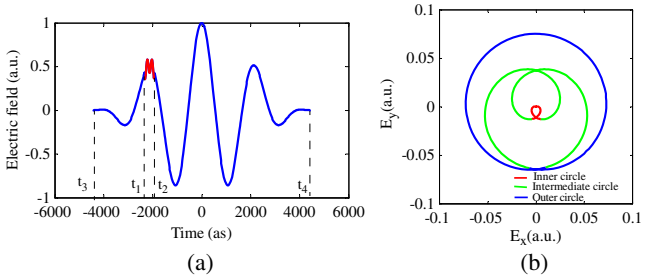

Fig. 1. (Color online) (a) Schematic illustration of the overlapping of an IAP (red line) with an IR pulse: time instants t_1 and t_2 determine the IAP, while t_3 and t_4 determine the IR pulse. (b) A typical electric field pattern of the overlapped IAP and the IR pulse, for which three categories of circles are defined: the inner circle, the intermediate circles, and the outer circle. $I_{\mathrm{IR}} = 2\times10^{14}$ W/cm^2, $I_{\mathrm{IAP}} = 8\times10^{11}$ W/cm^2.

It reflects the relative position of the IAP over the IR pulse, varying between zero and one. If the IAP location is close to the peak position of the IR pulse, η will approach zero; otherwise, it will approach one. In Fig. 2, the overlapped electric fields are plotted in the laser polarization plane for different overlapping parameters. The nine patterns correspond to five overlapping parameters: $\eta = 0, 0.2, 0.4, 0.6$, and 0.8. The duration of the IAP is $|t_2 - t_1|$.

In terms of the property of the induced photoelectron momentum distribution, the overall field patterns in Fig. 2 can be viewed as composed of four circles of different diameters. They are classified into three types: the inner circle ($\eta = 0.72$ to 1), the two intermediate circles ($\eta = 0.26$ to 0.72), and the outer circle ($\eta = 0$ to 0.26). On the inner circle, the overlapping IAP occupies a significant segment of the perimeter, making the IAP contribute more to the CEP effect; the outer circle induces momentum spectra with interference fringes.

Together, the strong IR and the relatively weak IAP pulses induce the hydrogen ionization because of the exponential dependence of the ionization rate on the overlapped electric fields. A hydrogen atom was employed in our simulation. Without considering the Coulomb interaction between the ionized electron and the nucleus[39], we deploy the strong field approximation (SFA)[40] to investigate the photoelectron momentum spectra induced by the overlapped pulses. The probability amplitude of the photoionized electron in the final continuum states with momentum $\overrightarrow{p}$ is

$$f(\overrightarrow{p}) = -i\int_{-\infty}^{\infty} \mathrm{d}t' \exp\left\{ i\int_{t'}^{\infty} \mathrm{d}t' \left[I_p + \frac{(\overrightarrow{p}+\overrightarrow{A})^2}{2} \right] \right\} \overrightarrow{d}(\overrightarrow{p}) \cdot \overrightarrow{E}, \tag{3}$$

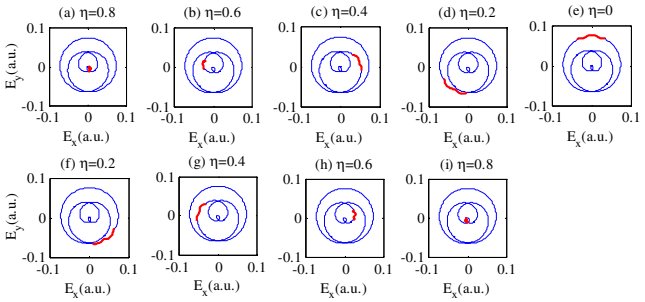

Fig. 2. (Color online) Electric field patterns of the superimposed IAP and IR pulse in the laser polarization plane for different overlapping parameters. The red curves indicate the superimposed segments. $I_{\mathrm{IR}} = 2\times10^{14}$ W/cm^2, $I_{\mathrm{IAP}} = 2\times10^{11}$ W/cm^2, and $\theta = \theta_{\mathrm{IR}} = 0$.

where $\overrightarrow{A}$ and $\overrightarrow{E}$ are the vector potential and the superimposed electric fields, respectively. I_p is the ionization threshold of the hydrogen atom (0.5 a.u.). The transition dipole moment for hydrogen $\overrightarrow{d}(\overrightarrow{p})$ has been computed as

$$\overrightarrow{d}(\overrightarrow{p}) = \frac{2^{3.5} \times (2I_p)^{\frac{5}{4}}}{\pi} [\overrightarrow{p}/(\overrightarrow{p}^2 + 2I_p)^3]. \quad (4)$$

Based on Eq. (3), a variety of photoelectron momentum spectra are computed for a range of overlapping parameters, and some typical spectra are shown in Fig. 3. It can be clearly observed that the momentum spectra can be classified into three categories, corresponding to the three classifications of the field patterns. Different overlapping positions result in entirely different momentum distributions. For overlapping parameter $\eta = 0.8$, the overlapped electric fields are around the center of the electric field pattern, shown as Figs. 2(a) and 2(i), thus, the photoelectron momentum spectra are also distributed around the center symmetrically. The induced momentum distribution is almost annular with two semilunes and a clear rotation. The maximum momenta are found approximately along the P_x-axis ($P_y = 0$). For $\eta = 0.4$ and 0.6, the overlapped electric field is a curve with a large curvature, distributed on the intermediate circles. Therefore, the photoelectron also shows the characteristic of the curve. The momentum spectra form irregular shapes. For overlapping parameter $\eta = 0$ and 0.2, the overlapped electric field is curved with a small curvature, so the momentum spectra form islands along either the P_y axis, the diagonal ($P_x = P_y$), or the anti-diagonal ($P_x = P_y$). This is the reason why the overlapped field pattern is viewed as composed of three types of circles (Sec. II). Of the three types of momentum distribution, the annular pattern possesses the most regular shape, therefore, $\eta = 0.72$ to 1 is chosen as the doable overlapping parameter range.

In order to verify the robustness of the doable overlapping parameter choice, eight simulated photoelectron momentum spectra for different initial phases of the IAP are presented in Fig. 4. One can clearly observe that the annular momentum patterns have all rotated a large angle for all of the initial IAP phase values. In detail, if θ is increased by $\pi/4$, the pattern will rotate an angle of approximately $\pi/4$. It implies that the CEP of an IAP is reflected in the photoelectron momentum distribution, which is a remarkable effect to exploit. In addition, one can also observe that the shape of annular momentum pattern remains unchanged after the rotation by θ. Therefore, the weight centers of the two district semilunes can be utilized as markings so that the rotation angle can be discerned clearly, which is fundamentally important for characterizing the IAP CEP. As depicted in Fig. 5(b), an arrow is drawn from the origin to the maximum momentum (the weight center of right semilune) to form the rotation angle $\theta_{\rm rot}$ with the P_x axis. Following this operation, the variation of the rotation angle versus the IAP CEP can be extracted, as shown in Fig. 5(a). It can be seen that this variation demonstrates an approximately linear relation. As is well known, a linear relation is the most robust measurement. Furthermore, the rotation period by our approach is 2π, compared to the angle of 0.63 reported in Ref. [27].

We now count the effect of the extreme CEP of the IR pulse, given the photoelectron momentum spectra generated by the overlapped fields for varying $\theta_{\rm IR}$ in Fig. 6. It

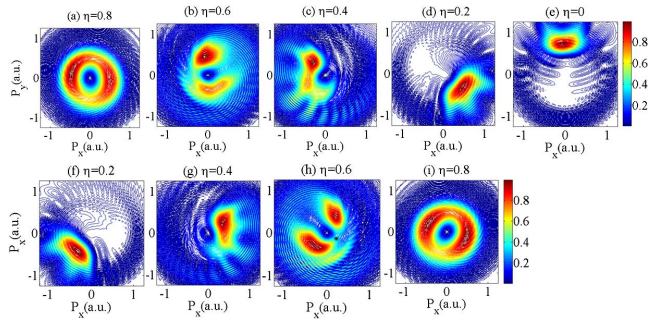

Fig. 3. (Color online) Photoelectron momentum spectra for different overlapping parameters. $I_{\rm IR} = 2 \times 10^{14}$ W/cm^2, $I_{\rm IAP} = 2 \times 10^{11}$ W/cm^2, $\theta = \theta_{\rm IR} = 0$.

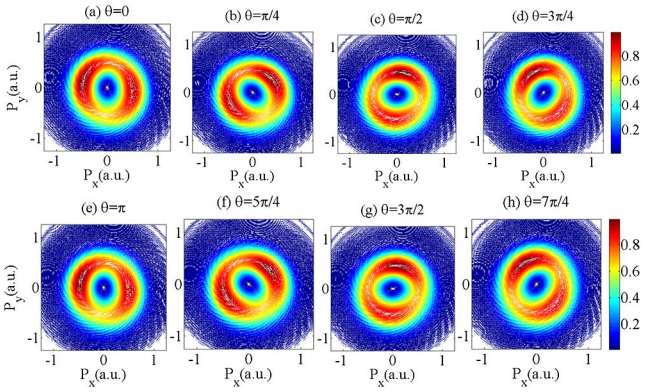

Fig. 4. (Color online) Photoelectron momentum spectra for different initial phases of the IAP: (a) $\theta = 0$, (b) $\theta = \pi/4$, (c) $\theta = \pi/2$, (d) $\theta = 3\pi/4$, (e) $\theta = \pi$, (f) $\theta = 5\pi/4$, (g) $\theta = 3\pi/2$, (h) $\theta = 7\pi/4$, and (i) $\theta = 2\pi$. The overlapping parameter η is set to be 0.8. $I_{\rm IR} = 2 \times 10^{14}$ W/cm^2, $I_{\rm IAP} = 2 \times 10^{11}$ W/cm^2, and $\theta_{\rm IR} = 0$.

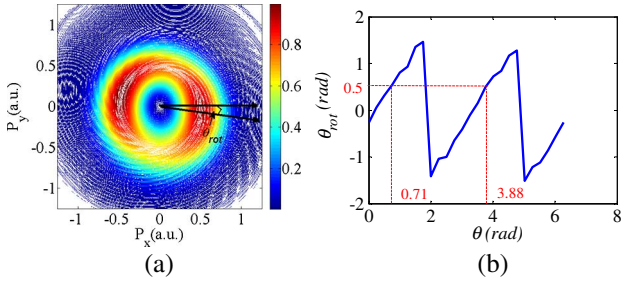

Fig. 5. (a) Rotation angle of the annular photoelectron momentum spectra versus the IAP CEP. (b) Schematic of the rotation angle of the annular photoelectron momentum spectra. The overlapping parameter η is 0.8. $I_{\rm IR} = 2 \times 10^{14}$ W/cm^2, $I_{\rm IAP} = 2 \times 10^{11}$ W/cm^2, and $\theta_{\rm IR} = 0$.

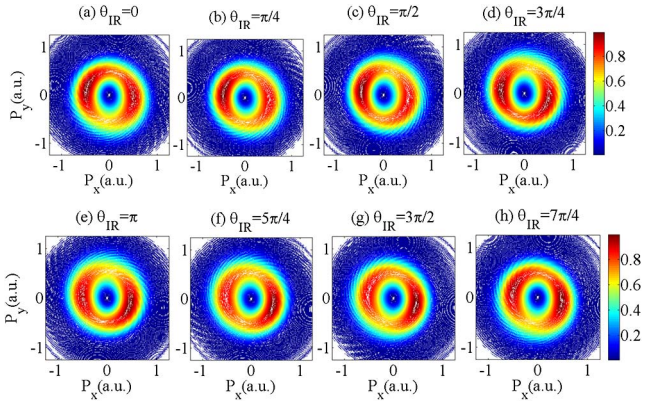

Fig. 6. Photoelectron momentum spectra with (a) $\theta_{IR} = 0$, (b) $\theta_{IR} = \pi/4$, (c) $\theta_{IR} = \pi/2$, (d) $\theta_{IR} = 3\pi/4$, (e) $\theta_{IR} = \pi$, (f) $\theta_{IR} = 5\pi/4$, (g) $\theta_{IR} = 3\pi/2$, (h) $\theta_{IR} = 7\pi/4$, and (i) $\theta_{IR} = 2\pi$. $I_{IR} = 2 \times 10^{14}$ W/cm^2, $I_{IAP} = 2 \times 10^{11}$ W/cm^2, $\eta = 0.8$, and $\theta = 0$.

is obvious that although θ_{IR} makes a change from 0 to 2π, the annular momentum patterns remain essentially unchanged. Therefore, the robustness of the proposed approach is corroborated[26,27].

Nevertheless, a drawback is shown in deploying the annular momentum spectra rotation; if two IAP CEPs differ by π, they cannot be distinguished. This is due to the symmetry of annular momentum spectra. In Fig. 5(a), one can see that for one particular rotation angle θ_{rot}, there will be two values for θ of the IAP CEP; for instance, the condition of $\theta_{rot} = 0.5$ gives $\theta = 0.71$ or 3.88. Thus, additional means are required to further distinguish IAP CEP values with a difference of π. To overcome this drawback, we can make use of the outer circle of the overlapped fields (Fig. 2) as a supplemental condition, as suggested in Ref. [24]. Judging by the polar distribution of the momentum spectra induced by the overlapped fields of the outer circle ($\eta = 0$), the IAP CEPs greater than π will have two convex points, while the ones less than π have three. For demonstration, the photoelectron momentum spectra for $\theta = 0.2\pi$ and $\theta = 1.2\pi$ are presented (Fig. 7). Obviously, it can be seen that the photoelectron momentum spectrum with $\theta = 1.2\pi$ has two convex points, and the one with $\theta = 0.2\pi$ has three. Therefore, this supplemental spectrum can distinguish two IAP CEPs differing by π.

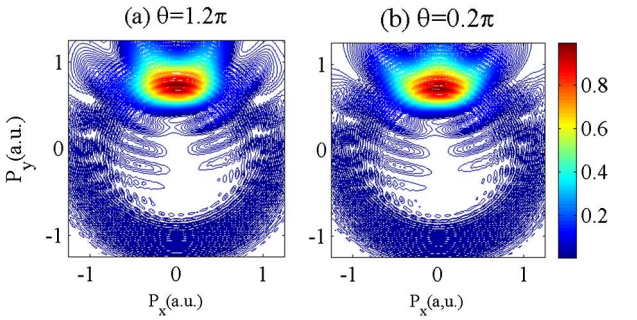

Fig. 7. Photoelectron momentum spectra with (a) $\theta = 1.2\pi$ and (b) $\theta = 0.2\pi$. $\eta = 0$ and $\theta_{IR} = 0$. $I_{IR} = 2 \times 10^{14}$ W/cm^2, and $I_{IAP} = 2 \times 10^{11}$ W/cm^2.

As mentioned above, the proposed method can further improve the performance of the IAP CEP characterization by optimizing the overlapping positions within the parameter interval of $\eta = 0.72$ to 1. In doing so, the regularity of the momentum distribution is to be considered first. Figure 8 demonstrates the photoelectron momentum spectra for different η. The six momentum patterns are all different, even though they are all induced by the inner-circle fields, which we classify (see Fig. 2). These momentum patterns can be divided into the symmetric and nonsymmetric ones. The symmetric patterns, as shown by Figs. 8(a)–8(d), display better regularity. In contrast, the nonsymmetric ones all manifest distorted patterns without rotational symmetry, as shown in Figs. 8(e)–8(f). The greater the overlapping parameter, the more regular the photoelectron momentum patterns are. In order to confirm that this law still holds for the situation of $\theta = \pi$, more momentum spectra are plotted in Fig. 9. These spectra demonstrate that they are

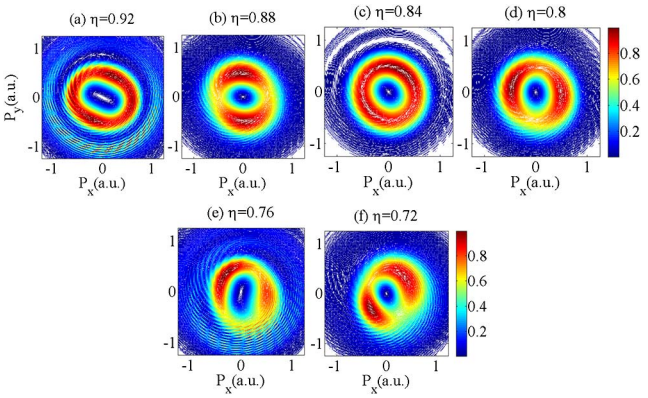

Fig. 8. Photoelectron momentum spectra for different overlapping parameters. (a) $\eta = 0.92$, (b) $\eta = 0.88$, (c) $\eta = 0.84$, (d) $\eta = 0.8$, (e) $\eta = 0.76$, and (f) $\eta = 0.72$. $I_{IR} = 2 \times 10^{14}$ W/cm^2, $I_{IAP} = 2 \times 10^{11}$ W/cm^2, and $\theta = \theta_{IR} = 0$.

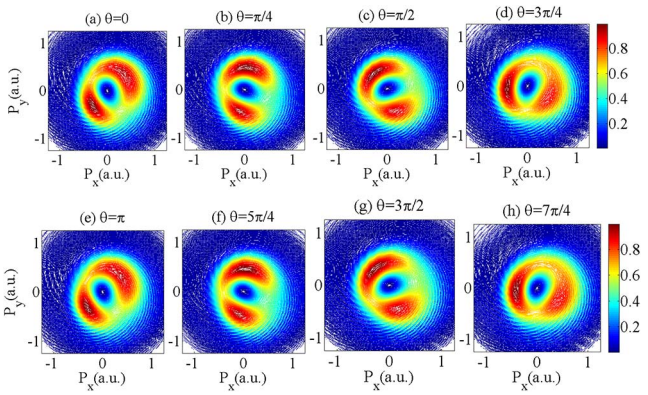

Fig. 9. Photoelectron momentum spectra for different initial phases of the IR pulse. (a) $\theta = 0$, (b) $\theta = \pi/4$, (c) $\theta = \pi/2$, (d) $\theta = 3\pi/4$, (e) $\theta = \pi$, (f) $\theta = 5\pi/4$, (g) $\theta = 3\pi/2$, (h) $\theta = 7\pi/4$, and (i) $\theta = 2\pi$. $\eta = 0.72$, $I_{IR} = 2 \times 10^{14}$ W/cm^2, $I_{IAP} = 2 \times 10^{11}$ W/cm^2, and $\theta_{IR} = 0$.

nonsymmetric for the small overlapping parameter $\eta = 0.72$. Eventually, our extensive search for the optimal overlapping parameters gives a result of $\eta = 0.86$, which optimizes the IAP CEP characterization

In conclusion, we numerically simulate the photoelectron momentum spectra of the hydrogen atom ionized by overlapped IAP and IR pulses in order to extract the CEP of the IAP. An overlapping parameter is defined to classify and choose the overlapping of the two pulses for obtaining the appropriate photoelectron momentum spectra, which can be deployed to get the CEP value. It is unveiled that, for the optimized overlapping parameter, the rotation angle of the momentum pattern shows an approximately linear relation with the CEP value, which is key to accurately characterizing the CEP. Compared with the existing methods, the accuracy and robustness of our strategy are both significantly improved. In addition, for two CEPs differing by π, a supplemental momentum spectrum can be utilized to unambiguously discern them. Thus, the present method can characterize the CEP of an IAP for a complete range of 0 to 2π.

This work was supported by the National Natural Science Foundation of China (Nos. 11674243 and 11674242) and the Fundamental Research Funds for the Central Universities (No. 3122016D029).

References

1. M. Hentschel, R. Kienberger, C. Spielmann, G. A. Reider, N. Milosevic, T. Brabec, P. Corkum, U. Heinzmann, M. Drescher, and F. Krausz, Nature **414**, 509 (2001).
2. A. Baltuška, T. Udem, M. Uiberacker, and M. Hentschel, Nature **421**, 611 (2003).
3. E. Goulielmakis, V. S. Yakovlev, A. L. Cavalieri, M. Uiberacker, V. Pervak, A. Apolonski, R. Kienberger, U. Kleineberg, and F. Krausz, Science **317**, 769 (2007).
4. H. Du, L. Luo, X. Wang, and B. Hu, Opt. Express **20**, 9713 (2012).
5. Q. Wang, Y. Zhang, Z. Wang, J. Ding, Z. Liu, and B. Hu, Chin. Opt. Lett. **14**, 110201 (2016).
6. J. Itatani, F. Quéré, G. Yudin, and M. Ivanov, Phys. Rev. Lett. **88**, 173903 (2002).
7. M. Kitzler, N. Milosevic, A. Scrinzi, F. Krausz, and T. Brabec, Phys. Rev. Lett. **88**, 173904 (2002).
8. M. F. Kling, Ch. Siedschlag, and A. J. Verhoef, Science **312**, 246 (2006).
9. P. M. Paul, E. S. Toma, and P. Breger, Science **292**, 1689 (2001).
10. D. J. Jones, S. A. Diddams, and J. K. Rankaetal, Science **288**, 635 (2000).
11. M. Kakehata, H. Takada, Y. Kobayashi, K. Torizuka, Y. Fujihira, T. Homma, and H. Takahashi, Opt. Lett. **26**, 1436 (2001).
12. C. Grebing, S. Koke, B. Manschwetus, and G. Steinmeyer, Appl. Phys. B **95**, 81 (2009).
13. E. Goulielmakis, V. S. Yakovlev, A. L. Cavalieri, M. Uiberacker, V. Pervak, A. Apolonski, R. Kienberger, U. Kleineberg, and F. Krausz, Science **317**, 769 (2007).
14. X. Chen, L. Canova, A. Malvache, A. Jullien, R. Lopez-Martens, C. Durfee, D. Papadopoulos, and F. Druon, Appl. Phys. B **99**, 149 (2010).
15. R. Kienberger, E. Goulielmakis, M. Uiberacker, A. Baltuska, V. Yakovlev, F. Bammer, A. Scrinzi, Th. Westerwalbesloh, U. Kleineberg, U. Heinzmann, M. Drescher, and F. Krausz, Nature **427**, 817 (2004).
16. M. Wen, L. L. Jin, H. Y. Wang, Z. Wang, Y. R. Lu, J. E. Chen, and X. Q. Yan, Phys. Rev. E **85**, 035401 (2012).
17. Q. Li, H. Chen, X. Zhang, and X. Yi, Chin. Phys. B **23**, 074206 (2014).
18. G. G. Paulus, F. Lindner, H. Walther, A. Baltuska, E. Goulielmakis, M. Lezius, and F. Krausz, Phys. Rev. Lett. **91**, 253004 (2003).
19. T. Wittmann, B. Horvath, W. Helml, M. G. Schätzel, X. Gu, A. L. Cavalieri, G. G. Paulus, and R. Kienberger, Nat. Phys. **5**, 357 (2009).
20. S. Micheau, Zh. Chen, and T. Morishita, J. Phys. B **42**, 065402 (2009).
21. T. Rathje, N. G. Johnson, M. Möller, F. Süßmann, D. Adolph, M. Kübel, R. Kienberger, M. F. Kling, G. G. Paulus, and A. M. Sayler, J. Phys. At. Mol. Opt. Phys. **45**, 074003 (2012).
22. V. V. Strelkov, E. Mevel, and E. Constant, Opt. Express **22**, 6239 (2014).
23. M. Miranda, Th. Fordell, C. Arnold, A. L'Huillier, and H. Crespo, Opt. Express **20**, 688 (2012).
24. Y. Xiang, J. Lu, Y. Niu, and S. Gong, J. Phys. B **48**, 135601 (2015).
25. G. Sansone and F. Kelkensberg, Nature **465**, 763 (2010).
26. L. Y. Peng, E. A. Pronin, and A. F. Starace, New J. Phys. **10**, 025030 (2008).
27. C. D. Liu, M. Reduzzi, A. Trabattoni, and A. Sunilkumar, Phys. Rev. Lett. **111**, 123901 (2013).
28. P.-L. He, C. Ruiz, and F. He, Phys. Rev. Lett. **116**, 203601 (2016).
29. A. Mancuso, D. Hickstein, and M. Dorney, Phys. Rev. A **93**, 053406 (2016).
30. A. Mancuso, M. Dorney, and D. Hickstein, Phys. Rev. Lett. **117**, 133201 (2016).
31. J. Wu, M. Magrakvelidze, L. P. H. Schmidt, M. Kunitski, T. Pfeifer, M. Schöffler, M. Pitzer, M. Richter, S. Voss, H. Sann, H. Kim, J. Lower, T. Jahnke, A. Czasch, U. Thumm, and R. Dorner, Nat. Commun. **4**, 2177 (2013).
32. A. N. Pfeiffer, C. Cirelli, M. Smolarski, R. Dörner, and U. Keller, Nat. Phys. **7**, 428 (2011).
33. M. Ivanovand and O. Smirnova, Phys. Rev. Lett. **107**, 213605 (2011).
34. M. Drescher, M. Hentschel, R. Kienberger, M. Uiberacker, V. Yakovlev, A. Scrinzi, Th. Westerwalbesloh, U. Kleineberg, U. Heinzmann, and F. Krausz, Nature **419**, 803 (2002).
35. M. Uiberacker, Th. Uphues, M. Schultze, A. J. Verhoef, V. Yakovlev, M. F. Kling, J. Rauschenberger, N. M. Kabachnik, H. Schröder, M. Lezius, K. L. Kompa, H.-G. Muller, M. J. J. Vrakking, S. Hendel, U. Kleineberg, U. Heinzmann, M. Drescher, and F. Krausz, Nature **446**, 627 (2007).
36. M. Schultze, M. Fieß, N. Karpowicz, J. Gagnon, M. Korbman, M. Hofstetter, S. Neppl, A. L. Cavalieri, Y. Komninos, Th. Mercouris, C. A. Nicolaides, R. Pazourek, S. Nagele, J. Feist, J. Burgdörfer, A. M. Azzeer, R. Ernstorfer, R. Kienberger, U. Kleineberg, E. Goulielmakis, F. Krausz, and V. S. Yakovlev, Science **328**, 1658 (2010).
37. K. Zhai, Z. Li, H. Xie, C. Jing, G. Li, B. Zeng, W. Chu, J. Ni, J. Yao, and Y. Cheng, Chin. Opt. Lett. **13**, 050201 (2015).
38. Y. Xie, Y. Yang, L. Han, Q. Yue, and C. Guo, Chin. Opt. Lett. **14**, 122601 (2016).
39. P. L. He, N. Takemoto, and F. He, Phys. Rev. A **91**, 063413 (2015).
40. W. T. Rhodes, in *Strong Field Laser Physics* (Springer, 2008), p. 162.